Applied Innovative Research
Vol. 1, March 2019, pp. 11-20

Structural, Optical, Photoluminescence and Electroluminescence Properties of Small ZnO Nanocrystals for Optoelectronic Device Applications

Anju Singh[1]* & H L Vishwakarma[2]

[1]Department of Physics, Rungta College of Engineering & Technology, Kohka Kurud Road, Bhilai 490 024, India
[2]Department of Physics, Government Engineering College, Jagdalpur 494 001, India

Received 19 September 2018; accepted 15 January 2019

In this study, zinc oxide (ZnO) has been prepared by chemical precipitation method using zinc acetate as precursor, poly vinyl pyrrolidone (PVP) as capping agent and deionised water as a solvent. X- ray diffraction (XRD), scanning electron microscopy (SEM), ultra violet visible (UV-Vis) absorption, photoluminescence (PL), and electroluminescence (EL) have been performed to characterize the structural, morphological and optical nature of the samples, respectively. X-Ray diffraction indicates that all of the as obtained samples have a pure phase (hexagonal wurtzite structure). Crystallite size has been calculated by Debye Scherrer formula and Lattice strain has been calculated by Williomson Hall equation. Cell volume, Lorentz factor, Lorentz polarization factor, lattice constants and crystal lattice distortion degree (R) and morphology index (MI) have also been studied. The average particle size has also been calculated by Brus equation by using UV-Visible absorption peak. An electroluminescence spectrum of ZnO nanocrystals has also been studied.

Keywords: Photoluminescence, Nanocrystals, Exciton binding energy, Absorption spectra, Morphology, Electroluminescence

Introduction

Zinc oxide (ZnO) exhibits many fascinating properties[1-7]. It is an intrinsic n-type semiconductor which belongs to II-VI group. It has a wide band gap of 3.37 eV at room temperature (RT). The exciton binding energy (60 meV) of ZnO is larger than those of the widely used semiconductors GaN (26 meV) or ZnSe (20 meV) and also larger than the RT thermal energy (25 meV). Because of these properties, ZnO presents a strong excitonic UV light emission at room temperature[2-6]. It also consist a high photoconductivity and considerable piezoelectric and pyroelectric properties[1]. ZnO has attracted much attention for potential applications in various electronic and optoelectronic devices due to their remarkable properties[7-21]. The electronic and optical properties of ZnO nanostructures depend on their size, shape and surface morphology[22,23]. Compared to nanoparticles, the one dimensional nanorod exhibits unique electronic and optical properties arising from their anisotropic geometry and large surface to volume ratio[24]. ZnO nanorod provides a direct conduction path along the direction of the c-axis for electron transport that reduces the number of grain boundaries greatly. The nanorods perform outstanding electron transportation capability[25-29]. ZnO is cheap and easily available material as compared to other oxide materials such as ZnO_2, Y_2O_3, Gd_2O_3, CeO_2 and Y_2SiO_5 etc.[30-36].

Various different physical or chemical synthetic approaches have been developed. Several reports on physical ZnO synthesis had been published which involves vapour phase oxidation[37], thermal vapour transport, condensation[38,39] methods and chemical vapour deposition[40]. These methods discussed above must be performed at high temperature (500-1500 ºC). On the other hand, chemical methods are of particular interest since they offer the potential of facile scale up at moderate temperature (100-200 ºC). Among these chemical methods precipitation[41-43], sol – gel[44-46] and micro emulsion[47] approaches are convenient and may lead to nanoparticles of controlled morphology. But in recent times much interest has been generated around the chemical route technique[48-50]. This technique is simple, cost effective, and reproducible and materials are readily available[51-57].

However, in spite of several decades of effort, some of the basic properties of ZnO still remain unclear[58,59]. In particular, the identification of the dominant intrinsic defects (oxygen vacancies, V_O, interstitial zinc, Zn_i, and hydrogen interstitials, H_i)[60-68] and the origins of the defect related emissions in the

*Corresponding author (E-mail: singh_nk24@yahoo.com)

visible region[69-78] have been controversial for quite a long time. The control of intrinsic defects and the corresponding effects on properties is of paramount importance in applications of ZnO.

In the photoluminescence (PL) spectra of ZnO, typically there are emission bands in the ultraviolet (UV) and visible (green, yellow, blue and violet) regions. The UV emission is usually considered as the characteristic emission of ZnO[79,80] and attributed to the band edge transition or the exciton combination[76]. Although the emission in the visible regions are universally considered to be associated with the intrinsic or extrinsic defects in ZnO, extensive controversies have existed for more than two decades on the clear defect centres and unambiguous electron transitions are not yet known in details[81]. For green emission, a number of different hypothesis have been proposed, such as transition between singly ionized oxygen vacancies and photo excited holes[69], transition between electrons close to the conduction band and deeply trapped holes at V_0^{++}, surface defects[70,75] etc. The yellow orange emissions have been assigned to interstitial oxygen and dislocation as well as Li dopants[58].

In the present study, we have synthesized the hexagonal structure ZnO nanocrystals using the zinc acetate organic precursor. The synthesized powder samples have been characterized using X – ray diffraction (XRD), UV – visible (UV – Vis) spectroscopy, scanning electron microscopy (SEM) and photoluminescence (PL) spectroscopy. The crystal structure, surface morphology and optical properties of the fine powders are critically examined. An electroluminescence spectrum of ZnO nanocrystals is also discussed.

Experimental

Materials

Zinc acetate dihydrate Zn $(CH_3COO)_2.2H_2O$, sodium hydroxide (NaOH) pallets, polyvinyl pyrrolidone (PVP) (Mwt 4000) and absolute ethanol were used to synthesize pure zinc oxide nanocrystals. All these chemicals were used as precursors which were obtained from Merck Chemical Company. PVP was used as a capping agent. In this experiment, all the glassware used was acid washed. The chemical reagents used were analytical reagent grade which needs no further purification. Ultrapure water was used for all dilutions and sample preparation. The whole synthesis process was done at room temperature.

Sample preparation

In a typical experiment, 2.2 g (0.2 mol/L) of zinc acetate Zn $(CH_3COO)_2.2H_2O$ was dissolved in 50 mL deionized water. The stirring rate of the solution was 1500 rpm and the process was conducted at room temperature. Then 1 g of PVP was dissolved in 50 mL deionized water and was added drop by drop to the constantly stirred solution for stabilizing the synthesized particles. The mixture was stirred at room temperature until a homogeneous solution was obtained. After that 0.4 g (0.2 mol/L) of 50 mL sodium hydroxide was added drop by drop to the above mixture which gave white voluminous precipitate. The stirring process was continued for 2 h till the white precipitate gets deposited at the bottom of the beaker. This solution was kept overnight for settlement of the precipitate. Then the precipitate was firstly washed 2 to 3 times with distilled water and then 1 to 2 times with absolute ethanol. After that the precipitate was filtered by using Whatmann filter paper. After this process the products were finally dried in a hot air oven at 100 °C for 1 h. The powder obtained was used for further characterization process.

Characterization

The crystal structure of the samples were investigated by X-Ray diffraction (XRD) using a XPERT-PRO diffractometer (Cu Kα radiation, λ=1.54056 Å) at 40 kV and 35 mA in the diffraction angle 2θ = 200 to 800. The morphology of the samples was characterized by the scanning electron microscopy (SEM) using JEOL-EO microscopy with accelerating voltage 20 kV. The optical absorption spectra of the particles were recorded using Perkin Elmer Lambda-45 spectrophotometer in the wavelength range of 200 to 800 nm. Photoluminescence (PL) data were collected using RF- 5301PC SHIMADZU spectrofluoro photometer with spectral slit width of 1.5 nm.

Formation of electroluminescence cell

The electroluminescence cell was prepared by using triple layer structure. In this cell nanoparticle emission layer were sandwiched between two electrodes. The transparent electrode has been prepared by depositing thin film of indium tin oxide (ITO) on clean glass substrate. This ITO coated glass behaves as an electrode. The surface resistivity of this electrode is 70-100 Ω/sq and L (Length) × W (Width) × T (Thickness) is about 75 mm × 25 mm × 1.1 mm. Then a mica sheet having window of 2×2 mm was

placed on the conducting glass plate so that window is on the film of ZnO sample. An aluminium foil strip was placed tightly over this window so as to have good contact with ZnO nanoparticle film and there is no air gap. The aluminium strip acts as second electrode (area 1 cm^2 and thickness ~100 Å). The layer of nanoparticle should be uniform and thin. Alternating voltage of various frequencies was applied and EL brightness (B) at different voltages (V) was measured with the help of photomultiplier tube along with corresponding current.

Results and Discussion

Structural studies

Figure 1 shows the XRD pattern of ZnO nanocrystals. The diffraction peaks indicate the nanocrystalline nature (JCPDS card no. 36 – 1451). These peaks at scattering angles (2θ) of 31.489, 34.135, 36.965, 47.267, 56.344, 62.616, 66.162, 67.717, 68.835 and 76.795 correspond to the reflection from (100), (002), (101), (102), (110), (103), (200), (112), (201) and (202) crystal planes, respectively. The XRD is identical to the hexagonal phase with wurtzite structure with space group (C6V = $P6_3mc$) and unit cell parameters a = b = 3.249 Å and c = 5.206 Å. These data is in good agreement with the data from Joint Committee of Powder Diffraction Standards (JCPDS 36-1451). No other diffraction peaks or other impurities have been found in the sample which also confirms that the product obtained is in pure phase. It is obvious that the XRD pattern appears many diffraction peaks and strong orientation peak at 2θ = 36.965º which is belong to (101) diffraction line.

The average crystalline size of the ZnO powder is estimated by the Scherrer's relation Eq. (1) given by[83].

$$D = \frac{k\lambda}{\beta \cos\theta} \quad \ldots (1)$$

Where D is crystalline size for (hkl) plane given in Table 2, k is a Sherrer's constant (which is 0.94 for Lorentzain line profiles and small crystals of uniform size), λ is the wavelength of the incident X-Ray radiation (CuKα = 0.154 nm or 1.54 Å), β is the full width at half maximum (FWHM) in radian and θ is the diffraction angle for (hkl) plane.

Micro strain is calculated by Williamson – Hall equation by using Eq. (2):

$$\beta \cos\theta = \frac{k\lambda}{D} + 4\varepsilon \sin\theta \quad \ldots (2)$$

Where β is the full width at half maximum (FWHM) of XRD peaks, k is Scherrer's constant, D is the crystalline size, λ is the wavelength of X-ray, ε is the lattice strain and θ is the Bragg's angle. The plot between βcosθ and 2sinθ along y and x axis shows linear extrapolation. The crystalline size is given by the intercept kλ/D and the strain ε is given by slope. Average crystallite size decreased the micro strain increased. This might be because of the mechanical

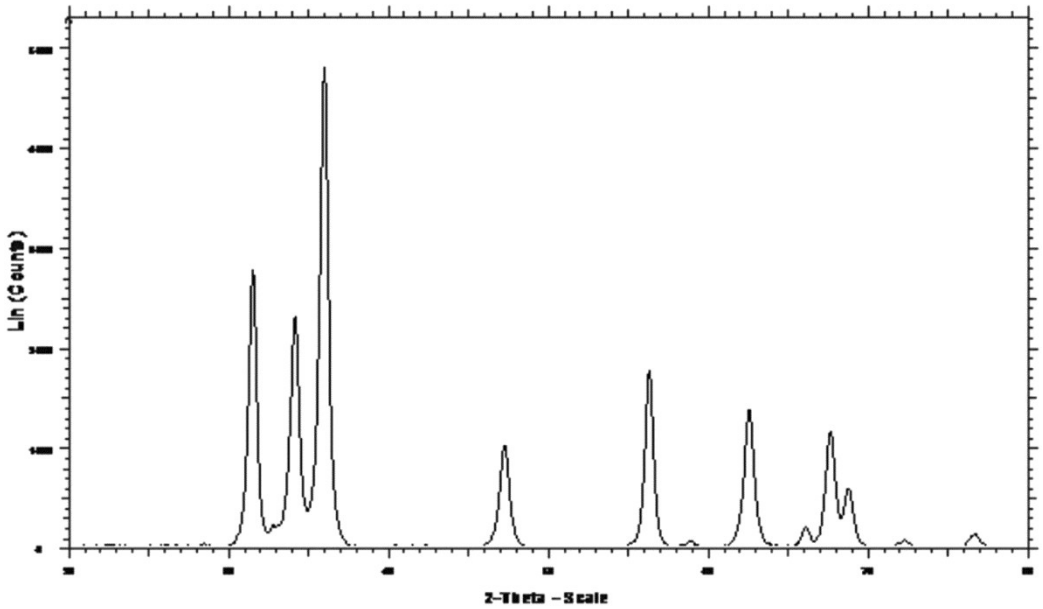

Fig. 1 – XRD pattern of ZnO nanocrystals.

surface-free energy of the metastable nanoparticles[84]. The calculated value of micro strain is given in Table 2.

The interplaner spacing (d) which is given in Table 1 has been evaluated using the Eq. (3) as explained by Mazhdi *et al.*[85].

$$\frac{1}{d^2}=\frac{4}{3}\left(\frac{h^2+hk+k^2}{a^2}\right)+\frac{l^2}{c^2} \quad \ldots (3)$$

Where a and c is the lattice constants which are defined by Eqs (4) and (5) given in Table 1:

$$a=\frac{\lambda}{\sqrt{3}\sin\theta} \cdot \quad \ldots (4)$$

For (101) plane the lattice constant a has been calculated by using Eq. (4) as explained by cullity *et al.*[83] is found to be a= 2.807 Å while:

$$c=\frac{\lambda}{\sin\theta} \quad \ldots (5)$$

Similarly for (101) plane the lattice constant c has been calculated by using Eq. (5) as explained by Cullity *et al.*[83] and found to be c=4.861 Å. Hence the ratio c/a =1.73174 shown in Table 1.

Volume is calculated by Eq. (6) which is given by[86], shown in Table 2.

$$V=\frac{\sqrt{3}}{2}a^2c=0.866a^2c \quad \ldots (6)$$

The crystal lattice distortion degree (R) is shown in Table 2 can be calculated by Eq. (7) which is given by[87].

$$R=\left[2a\left(\tfrac{2}{3}\right)\tfrac{1}{2}\right]c \quad \ldots (7)$$

Units Morphology Index (MI) is developed from FWHM of XRD data. The FWHM of two peaks are related with MI to its particle morphology. MI is obtained from Eq. (8).

$$M.I=\frac{FWHM_h}{FWHM_h+FWHM_p} \cdot \ldots (8)$$

Where MI is morphology index, $FWHM_h$ is highest FWHM value obtained from peaks and $FWHM_p$ is value of particular peak's FWHM for which MI is to be calculated[88] given in Table 2. The Lorentz-polarization factor is most important of the experimental quantities that control X-ray intensity with respect to diffraction angle. In the intensity calculations Lorentz factor is combined with the polarization factor and further the variation of the Lorentz's factor with the Bragg angle (θ) is shown[89-91]. The overall effect of Lorentz factor is to decrease the intensity of the reflections at intermediate angles compared to those in the forward or backward directions. Lorentz factor and Lorentz Polarization factor are calculated from Eqs (9) and (10) which is given in Table 2:

$$\text{Lorentz factor}=\frac{\cos\theta}{\sin^2 2\theta}=\frac{1}{4\sin^2\theta\cos\theta} \quad \ldots (9)$$

$$\text{Lorentz polarization factor}=\frac{1+\cos^2 2\theta}{\sin^2\theta\cos\theta} \quad \ldots (10)$$

Table 1 – Lattice constants a and c, c/a ratio and d-spacing.

hkl	2θ	Lattice constant *a* (Å)	Lattice constant *c* (Å)	c/a	d-spacing (Å)
100	31.489	3.278	5.679	1.7324588	2.83875
002	34.135	3.031	5.251	1.7324315	2.62458
101	36.965	2.807	4.861	1.7317421	2.49508
102	47.267	2.219	3.844	1.7323118	1.92149
110	56.344	1.884	3.264	1.7324841	1.63159
103	62.616	1.712	2.966	1.7324766	1.48239

Table 2 — Crystalline size (D), lattice distortion degree (R), volume (V), micro strain, morphology index, Lorentz factor and Lorentz polarization factor.

Crystalline size (D) (nm)	Lattice distortion degree (R)	Volume (V) $(Å)^3$	Micro strain (βcosθ)	Morphology index (MI)	Lorentz factor	Lorentz polarization factor
14.86	0.12410508	52.854	0.54446	0.54649	3.52794	24.37335
14.64	0.10610521	43.368	0.60334	0.54119	3.03609	21.20350
15.33	0.09096551	33.169	0.52781	0.55053	2.62297	17.19015
13.39	0.05686557	16.391	0.53817	0.50835	1.69807	7.105024
15.52	0.04099584	10.033	0.52109	0.53557	1.27233	6.652447
13.89	0.03385195	7.528	0.58241	0.5	1.08368	5.251748

Morphological studies

The surface morphology of the synthesized ZnO nanoparticles was investigated by SEM micrograph which is shown in Fig. 2 with different magnification. SEM image as shown in Fig. 2 shows hexagonal type structure of the synthesized ZnO nanocrystals. The prominent well structured growth observed from SEM micrograph of the fine particles confirms the development of hexagonal wurtzite crystal structure of the ZnO nanocrystals. It may be noted that the grain size of the ZnO fine powders evaluated from SEM is in good agreement with the particle size calculated from XRD analysis. The SEM image represents the agglomeration and cluster form of particles and also with narrow particle size distribution. The synthesized ZnO powder size investigated was in different shapes like rods, sheets and spherical particles.

Optical properties

The optical absorption spectra of ZnO are measured in the range of 200-800 nm. The UV-Visible absorption spectra of ZnO nanocrystals in deionised water solvent show an excitonic absorption peaks 225 nm, 330 nm, 340 nm, 355 nm and 375 nm. These spectra were taken at room temperature, the ZnO nanocrystals sample exhibit salient exciton absorption features due to the relatively large binding energy of exciton (60 meV). The absorption peak exhibits a blue shift. When photons of the higher energy states are greater than the band gap of the semiconductor, an electron is transferred from the valance band to the conduction band[92]. Due to this reason an abrupt increase in the absorbency of the material to the wavelength corresponding to the band gap energy. It is clear from the Fig. 3; the spectrum reveals a characteristic maximum absorption peak at wavelength of 375 nm which can be assigned to the intrinsic band gap absorption of ZnO due to the electron transition from the valance band to the conduction band. These sharp peaks show that the particles are in nanosize and the particle size distribution is narrow.

Typical exciton absorption at 375 nm is observed in the absorption spectrum at room temperature, which is blue shifted with respect to the bulk absorption edge appearing at 380 nm[98] at room temperature. It is clear that the absorption edge systematically shifts to the lower wavelength or higher energy with decreasing size of the nanoparticle. This pronounced a systematic shift in the absorption edge is due to the quantum size effect.

For further confirmation, the particle size of the ZnO nano powder was also estimated by optical method using Brus Eq. (11) given by[93]:

$$E^{eff} = E_g + \frac{h^2\pi^2}{2\mu R^2} - \frac{1.8e^2}{4\pi\varepsilon'\varepsilon_0 R} \quad \ldots (11)$$

With $\left(1/\mu\right) = \frac{1}{me^*} + \frac{1}{mh^*}$

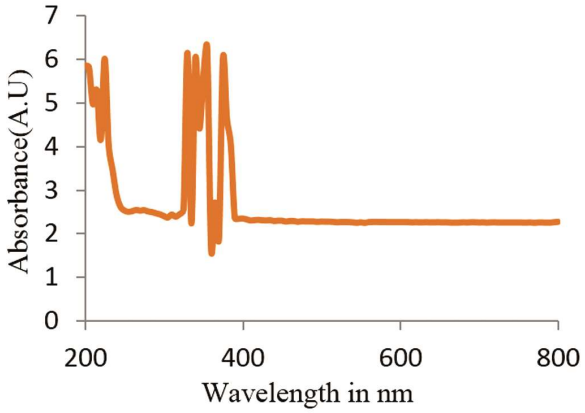

Fig. 3 – UV-Visible absorption spectra of ZnO nanocrystals.

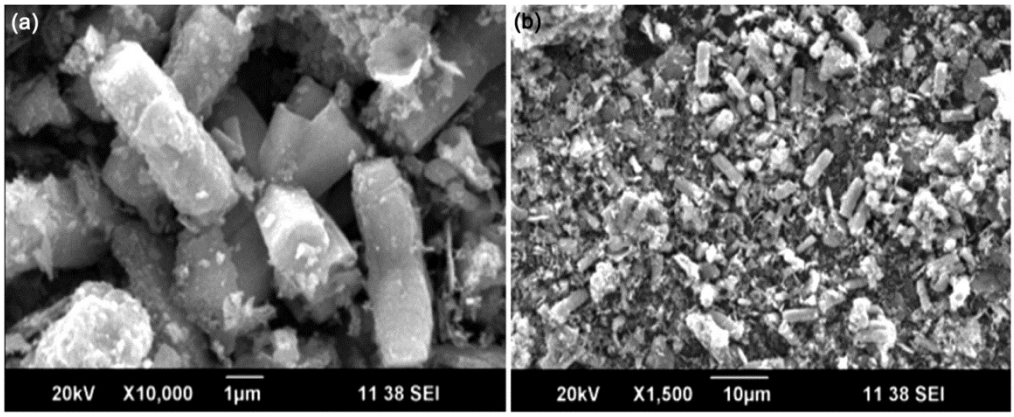

Fig. 2 – SEM image of ZnO nanocrystals at (a) high and (b) low magnification.

Where me* is the effective mass of the electron (0.19 me), mh* is the effective mass of the hole (0.8 mh), R is the radius of the particle, ε′ is the dielectric constant (5.7) and ε_0 is the permittivity of free space. The particle size of the ZnO nanopowder calculated using Brus equation was found to be 3.3 nm which is not good agreement with the size of 14 nm calculated from XRD analysis.

Furthermore, the optical bandgap of the synthesized ZnO nanocrystals was critically examined near the materials fundamental absorption band edge using the Urbach Eq. (12) given by[94]:

$$\alpha h\nu = A(h\nu - Eg)^m \quad \ldots (12)$$

Where, α is the absorption coefficient, A is a constant which is independent from photon energy, $h\nu$ is the energy of incident photons and exponents n whose value depends upon the type the transition which may have values 1/2, 2, 3/2 and 3 corresponding to the allowed direct, allowed indirect, forbidden direct and forbidden indirect transitions, respectively. Figure 4 show the variation of $(\alpha h\nu)^2$ versus photon energy, $h\nu$ for ZnO nanopowder with n values of 1/2. Allowed direct band gap of ZnO nanoparticles is calculated to be 5.3 eV, which is higher than reported value 3.5 eV. The increase in the band gap of the ZnO nanoparticles with the decrease in particle size may be due to a quantum confinement effect.

According to quantum confinement theory, as a particle size decreases comparable to the wavelength of the electron, the electron out of its interaction with that particle gets confined to discrete quantum energy levels, which will give rise to an enlargement in the energy band gap[95-97]. Therefore, the increased band gap energy of our ZnO nanocrystals is due to decrease in their particle size to nano order and the above described quantum size effect according to the quantum confinement theory. It also confirms that the increase in band gap to the order of 5.3 eV is due to the quantum size effect. That is, because of the decrease in size of the ZnO particle to nano order, comparable to the wavelength of electrons, the electrons interact with the ZnO and get confined into quantum energy levels. This leads to increase in the band gap of the ZnO nanoparticles and hence the blue shift in the absorbance spectrum.

Photoluminescence studies

Figure 5 shows room temperature photoluminescence spectra from ZnO powder samples over wavelength range 400-700 nm on irradiating at wavelength λ_{ex} = 265 nm. The photoluminescence spectroscopy is an excellent intensive technique for the investigation of the exact band edge transition levels of semiconductor materials. It is worth mentioning that the physical properties of semiconducting materials undergo changes when their dimensions get down to nanometer scale known as quantum size effect. For example quantum confinement increases the band gap energy of ZnO, which has been observed from photoluminescence. The photoluminescence originates from the recombination of surface states. The strong PL peak implies that the surface states remain very shallow, as it is reported that quantum yields of band edge will decrease exponentially with increasing depth of surface state level. In pure ZnO PL spectrum, a sharp green emission band at 531 nm which is also known as a deep level emission, relates to the deep level states. Singly ionized oxygen vacancy is responsible for this emission in ZnO. The visible emission is caused by the radiative recombination of a photo generated hole with an electron occupying oxygen vacancy. Further the spectrum also reveals the narrow size distribution of nanoparticles in the powder as the luminescence peak full width half maximum (FWHM) is only in few nanometers.

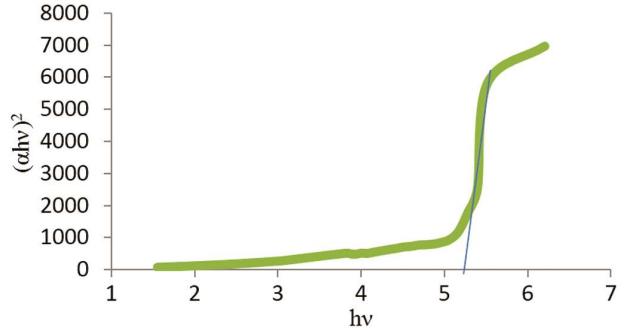

Fig. 4 – Plot of $(\alpha h\nu)^2$ versus photon energy ($h\nu$) for ZnO nanocrystals.

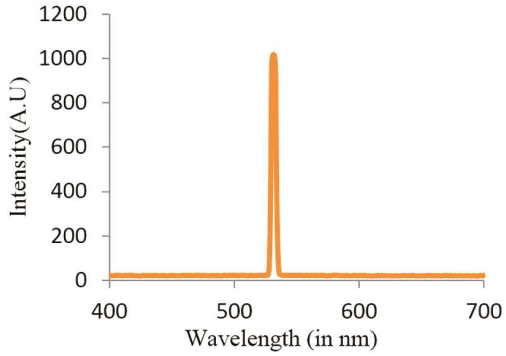

Fig. 5 – Photoluminescence spectra of ZnO nanocrystals.

However, the physical mechanism behind visible light emission in ZnO is claimed by different authors in different ways and is still under controversy. Therefore, it is important to investigate the luminescent mechanism caused by the defects of ZnO thin films, since they are the key factors for obtaining the visible luminescence.

The energy band gap (Eg) and crystal size for ZnO NPs from PL spectrum calculated by using Eqs (13) and (14):

$$Eg(eV) = \frac{1240}{\lambda_{nm}} \quad \ldots (13)$$

Crystal size (diameter=2r) was then calculated from energy gap using Eq. (14).

$$E_{NP} = E_{gbulk} + \frac{\hbar^2 \pi^2}{2er^2 m_o}\left(\frac{1}{m_e} + \frac{1}{m_h}\right) - \frac{1.8e}{4\pi\varepsilon\varepsilon_o r} \quad \ldots (14)$$

where E_{NP} is NPs band gap, E_{gbulk} is the bulk band gap, m_e is the electron effective mass (=0.26 for ZnO), m_h is the hole effective mass (=0.59 for ZnO), e is the electron charge, r is the radius of quantum dot, m_0 is the free electron mass, ε_0 is the permittivity of free space and ε is the relative permittivity.

Electroluminescence studies

Effects of temperature, film thickness and morphology on the electroluminescence (EL) have been studied. An EL spectrum had been observed at different frequencies.

Effect of temperature

It is well known that increase in temperature produces greater size of the phosphor particles. If the particle size is greater we will get poor EL brightness.

Effect of film thickness

The brightness of an EL device is a function of the applied electric field. The brightness can be strongly affected by the layer thickness. This suggests that using small phosphor powder particles, i.e., reduced thickness of the emitting layer would result in high brightness. For this reason an emitting layer as thin as possible was fabricated i.e. one monolayer of phosphor particles.

Effect of morphology

The morphology of ZnO changes at higher temperature (above 1000 ºC). Below this temperature ZnO particles have a hexagonal (wurtzite) structure while a cubic structure is obtained if heated above 1000 ºC. The crystal structure plays an important role for EL characteristics. It is also interesting that the wurtzite structure of the phosphor is responsible for the EL properties not the cubic structure. If the phosphor is made below 1000 ºC the phosphor crystallizes in a wurtzite structure but has particle size less than 20 µm, which again produces good EL characteristics.

Effect of voltage on current density

The voltage current density characteristics of ZnO at frequencies of 800 Hz, 1000 Hz and 1200 Hz are shown in Fig. 6 (a-c). It is clear from the observation made that as the input voltage increases there is

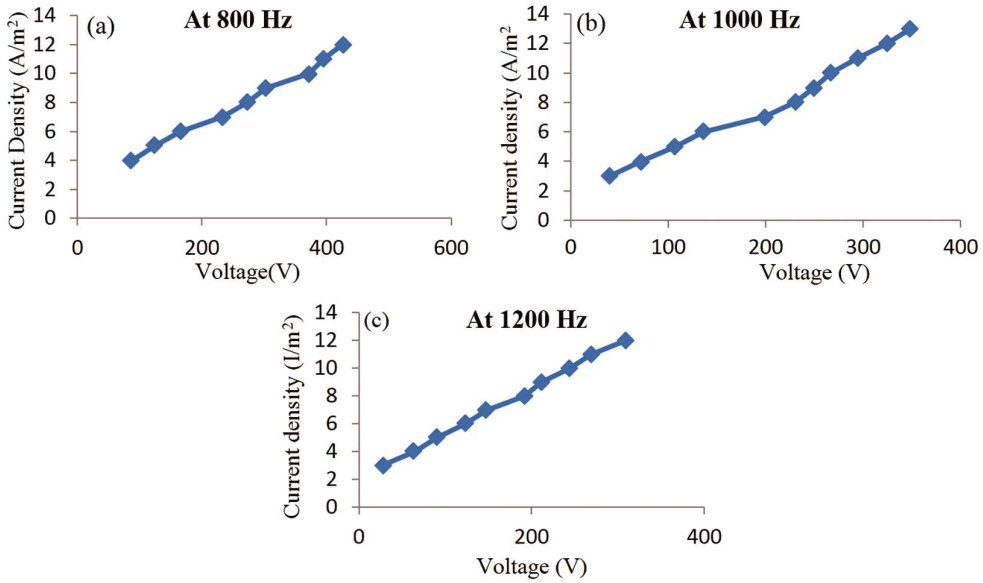

Fig. 6 – Effect of voltage on current density at different frequencies of (a) 800 Hz, (b) 1000 Hz and (c) 1200 Hz.

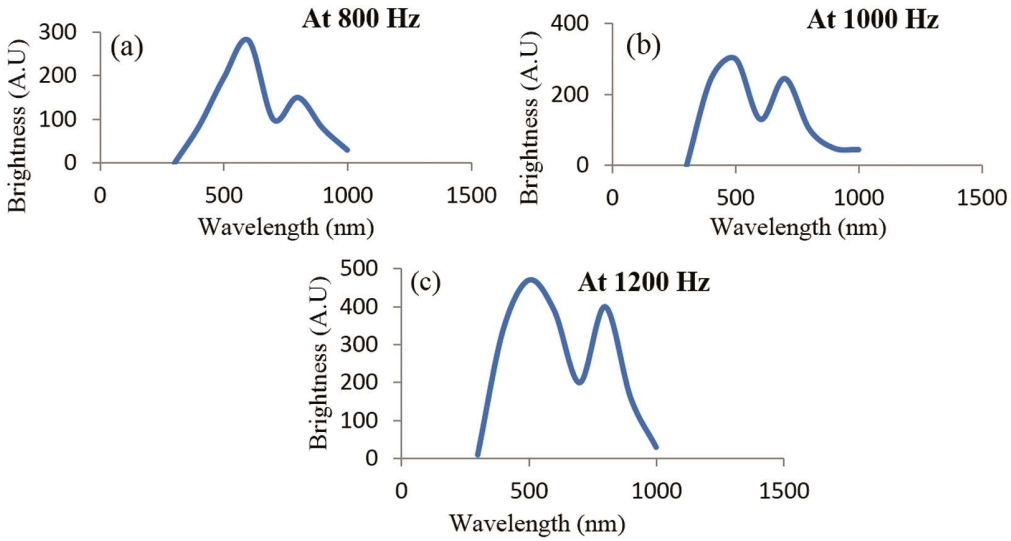

Fig. 7 – Electroluminescence spectra of ZnO at the frequency of (a) 800 Hz, (b)1000 Hz and (c) 1200 Hz.

continuous increases in current density. In the present study linear relation is obtained between voltage and current density. This indicates the ohmic nature of impedance. In this model, carriers tunnel across an energy barrier into the valance band and electrons tunnels across the conduction band of nanoparticles. These carriers are transported through a series of field associated ionization steps.

Electroluminescence spectra

The EL spectra of ZnO samples at excitation frequency of 800, 1000 and 1200 Hz is shown in Fig. 7 (a-c). The EL spectra at frequency of 800 Hz show two different peaks of 600 nm (yellow) and 800 nm (red) which is obvious from Fig. 7 (a). At 1000 Hz two different peaks of 500 nm (green) and 700 nm (red) are observed from Fig. 7 (b). Similarly from Fig. 7 (c), at 1200 Hz two another peaks 500 nm (green) and 800 nm (red) are observed. It is important to mention that due to the broad peak emission range of 400 -800 nm, a bright white light is clearly observed by the naked eye. These peaks are due to different deep level defects namely V_O, V_{Zn} and oxygen anti-site (O_{Zn}) in the ZnO small rods. Our EL spectra also show that the peak positions have shifted. When voltage is increased, more electrons and holes are injected into the emission layer. The recombination of electrons and holes, the brightness is increased with increasing voltage. The EL brightness with variation of voltage is agreement with excitation – collision mechanism and formation of Mott-Schottky barrier. The electroluminescent efficiency depends on the carrier life time of the injection charge carriers. The brightness can be strongly affected by the layer thickness. This suggests that using smaller phosphor powder particles (i.e., reduced thickness of emitting layer) results in high brightness.

Conclusions

This study focuses on the synthesis, structural, morphological and optical characterization of pure zinc oxide small rods. Pure zinc oxide nanoparticles have a hexagonally crystalline structure. XRD study reveals better crystallization of the powder. The particle size varies from 13-15 nm. It has been seen that the growth orientation of the prepared ZnO was (101). SEM image indicates agglomeration of the particles. The Scanning Electron Microscope (SEM) image confirmed the size and shape of these nanocrystals. The PL spectra shows peak in green region around 531 nm. The peak at 531 nm originates from the singly ionized oxygen vacancy.

The visible emission is caused by the radiative recombination of a photo generated hole with an electron occupying oxygen vacancy. The optical band gap value of the synthesized ZnO small rods is found to be 5.3 eV from the absorption spectroscopy. The UV- visible absorption spectra of ZnO in deionised water solvent show an excitonic absorption peaks 225 nm, 330 nm, 340 nm, 355 nm and 375 nm. Optical absorption analysis of the sample exhibits a blue shift in the absorption band edge. EL studies shows that light emission starts from ZnO at lower threshold voltage and higher EL intensity is obtained in case of smaller particles. Thus high efficiency EL devices for display and lightening can be fabricated by using

small size of ZnO rods. This study provides new approaches to change the optical properties which can be used as a strong tool for further optoelectronic applications.

Acknowledgement

The authors are thankful to the SAIF Kochi, Ernakulum, for characterization of samples by SEM and XRD technique and Rani Durgawati University for UV-Vis absorption spectra and EL of the given samples.

References

1 Wang Z & Song J, *Science*, 312 (2006) 242.
2 Tang Z, Wang G, Yu P, Kawasaki M, Ohtomo A, Koinuma H & Segawa Y, *Appl Phys Lett*, 72 (1998) 3270.
3 Bilecka I, Elser P & Niederberger M, *ACS Nanomater*, 3 (2009) 467.
4 Qurashi A, Tabet N, Faiz M & Yamzaki T, *Nanoscale Res Lett*, 4 (2009) 948.
5 Chen H, Wu X, Gong L, Ye C, Qu F & Shen G, *Nanoscale Res Lett*, 5 (2010) 570.
6 Dharai S & Giri P, *Nanoscale Res Lett*, 6 (2011) 504.
7 Balti I, Mezni A, Dakhlaoui – Omrani A, Leone P, Viana B, Brinza O, Smiri L & Jouini N, *J Phys Chem C*, 115 (2011) 15758.
8 Dietl T, Ohno H, Matsukara F, Cibert J & Ferrand D, *Science*, 287 (2000) 1019.
9 Zhou S, Liu L, Yuan H, Chen X, Lou S, Hao Y, Yuan R & Li N, *Nanoscale Res Lett,* 5 (2010) 1284.
10 Shi H & Duan Y, *Nanoscale Res Lett*, 4 (2009) 480.
11 Zhou S, Yuan H, Liu L, Chen X, Lou S, Hao Y, Yuan R & Lin X, *Appl Phys A*, 102 (2011) 367.
12 Yang H, Yu S, Lau S, Herng T & Tanemura M, *Nanoscale Res Lett*, 5 (2010) 247.
13 Fukumura T, Jin Z, Ohtomo A, Koinuma H & Kawasaki M, *Appl Phys Lett*, 75 (1999) 3366.
14 Zeng X, Yuan J & Zhang L, *J Phys Chem C*, 112 (2008) 3503.
15 Barick K, Aslam M, Dravid V & Bahadur D, *J Phys Chem C*, 112 (2008) 15163.
16 Liu Z, Zhang Q, Shi G, Li Y & Wang H, *J Magn Mater*, 323 (2011) 1022.
17 Duah L, Zhao X, Liu J, Geng W, Xie H & Chen S, *J Magn Mater*, 323 (2011) 2374.
18 Mi W, Bai H, Liu H & Sun C, *J Appl Phys*, 101 (2007) 023904.
19 Liu J, Wang K, Yu M & Zhou W, *J Appl Phys*, 102 (2007) 024301.
20 Cheng X & Chien C, *J Appl Phys*, 93 (2003) 7876.
21 Yoon S W, Cho S B, We S C, Yoon S, Suh B J, Song H K & Shin Y J, *J Appl Phys*, 93 (2003) 7879.
22 Li Q, Li H, Wang R M, Li G F, Yang H & Chen R, *J Alloys Comp*, 567 (2013) 1.
23 Li Q, Chen Y Q, Luo L B, Wang L, Yu Y Q & Zhai L, *J Alloys Comp*, 560 (2013) 156.
24 Wu H N, Xue M S, Ou J F, Wang F J & Li W, *J Alloys Comp*, 565 (2013) 85.
25 Jung J, Myoung J & Lim S, *Thin Solid Films*, 520 (2012) 5779.
26 Chang C M, Hon M H & Leu I C, *Sens Actuator B Chem*, 151 (2010) 15.
27 Poudel P & Qiao Q Q, *Nanoscale*, 4 (2012) 2826.
28 Huang Q, Fang L, Chen X & Saleem M, *J Alloys Comp*, 509 (2011) 9456.
29 Ling T, Song J G, Chen X Y, Yang J, Qiao S Z & Du X W, *J Alloys Comp*, 546 (2013) 307.
30 Dubey V, Agrawal S & Kaur J, *Int J Light Electron Opt*, 126 (2015) 1.
31 Tamrakar R K, Upadhyay K & Bisen D P, *J Rad Res Appl Sci*, 7 (2014) 526.
32 Tamrakar R K, Bisen D P, Upadhyay K & Bramhe N, 1 (2014) 23.
33 Tiwari N, Kuraria R K & Tamrakar R K, *J Rad Res Appl Sci*, 7 (2014) 542.
34 Tamrakar R K, Research on *Chemical Intermediates,* (2013) http://dx.doi.org/10.1007/s11164-013-1166-4.
35 Tamrakar R K & Bisen D P, *Res Chem Intermed*, 39 (2013) 3043.
36 Tamrakar R K, Bisen D P, Robinson C S, Sahu I P & Brahme N, *Indian J Mater Sci*, 7 (2014) 396147.
37 Hu J Q, Li Q, Wong N B, Lee C S & Lee S T, *Chem Mater*, 14 (2002) 1216.
38 Lao J Y, Huang J Y, Wang D Z & Ren Z F, *Nano Lett*, 3 (2003) 235.
39 Lao J Y, Wen J G & Ren Z F, *Nano Lett*, 2 (2002) 1287.
40 Wu J J & Liu S C, *J Phys Chem B*, 106 (2002) 9546.
41 Pesika N S, Hu Z, Stebe K J & Searson P C, *J Phys Chem B*, 106 (2002) 6985.
42 Radovanovic P V, Norberg N S, Mcnally K E & Gamelin D R, *J Am Chem Soc*, 124 (2002) 15192.
43 Seelig E W, Tang B, Yamilov A, Cao H & Chang R P H, *Mater Chem Phys*, 20 (2003) 257.
44 Bandyopadhyay S, Paul G K, Roy R, Sen S K & Sen S, *Mater Chem Phys*, 174 (2002) 83.
45 Hoyer P & Weller H, *J Phys Chem*, 99 (1995) 14096.
46 Paul G K, Bandyopadhyay S, Sen S K & Sen S, *Mater Chem Phys*, 79 (2003) 71.
47 L Guo, Y L Ji, H Xu, P Simon & Z Wu, *J Am Chem Soc*, 124 (2002) 14864.
48 Ezema F I & Okeke C E, *GJST*, 3 (2002) 90.
49 Ezema F I, Ekwealor A B C & Ji R U, *J Optoelectron Adv Mater*, 19 (2007) 1898.
50 Eya D D O, Ekpunob A J & Okeke C E, *Pac J Sci Technol*, 6 (2005) .
51 Dubey V, Tiwari R, Tamrakar R K, Rathore G S & Chitrakat S, *Infrared Phys Technol*, 67 (2014) 537.
52 Tamrakar R K, Bisen D P, Upadhyay K & Tiwari S, *J Radiat Res Appl Sci*, (2014).
53 Tamrakar R K, Upadhyay K & Bisen D P, *J Radiat Res Appl Sci*, (2014).
54 Tiwari N, Kuraria R K & Tamrakar R K, *J Radiat Res Appl Sci*, (2014).
55 Vijayan T A, Chandramohan R, Valanarasu S J, Thirumalai S, Venkateswaran T, Mahalim S R & Hrikumar S, *Sci Technol Adv Mater*, 9 (2008) 035007.
56 Widiyastuti W, Maula I, Nurtono T, Taufany F, Machmudah S, Winardi S & Panatarani C, *Chem Eng J*, 254 (2014) 252.
57 Yang Y, Wang X H, Sun C K & Li L T, *J Appl Phys*, 105 (2009) 094304.

58 O¨zgu¨r U, Alivov Y, Liu C, Teke A, Reshchikov M, Dogan S, Avrutin V, Cho S & Morkoc H, *J Appl Phys*, 98 (2005) 041301.
59 Schmide-Mende L & MacManus-Driscoll J L, *Mater Today*, 10 (2007) 40.
60 Hagemark K I & Chacha L C, *J Solid State Chem*, 15 (1975) 261.
61 Mahan G D, *J Appl Phys*, 54 (1983) 3825.
62 Kro¨ger F A, *The Chemistry of Imperfect Crystals*, 2nd Edn North Holland, Amsterdam (1974).
63 Gavryushin V, Rac˘iukaitis G, Juodz˘balis D, Kazlaulskas A & Kubertivic˘ius V, *J Cryst Growth*, 138 (1994) 924.
64 Look D C & Hemsky J W, *Phys Rev Lett*, 82 (1999) 2552.
65 Tuomisto F, Ranki V, Saarinen K & Look D C, *Phys Rev Lett*, 91 (2003) 205502.
66 Look D C, Falow G C, Reunchan P, Limpijumnong S, Zhang S B & Nordlund K, *Phys Rev Lett*, 95 (2005) 225502.
67 Van de Walle C G, *Phys Rev Lett*, 85 (2000) 1012.
68 Janotti A & Van de Walle C G, *Nat Mater*, 6 (2007) 44.
69 Vanheusden K, Seager C H, Warren W L, Tallant D R & Voigt J A, *Appl Phys Lett*, 68 (1996) 403.
70 Zhang S B, Wei S H & Zunger A, *Phys Rev B*, 63 (2001) 075205.
71 Kang H S, Kang J S, Kim J W & Lee S Y, *J Appl Phys*, 95 (2004) 1246.
72 Dingle R, *Phys Rev Lett*, 23 (1969) 579.
73 Dietz R E, Kamimura H, Sturge M D & Yariv A, *Phys Rev*, 132 (1963) 1559.
74 Kimpel B M & Schulz H J, *Phys Rev B*, 43 (1991) 9938.
75 Studenikin S A, Golego N & Cocivera M, *J Appl Phys*, 84 (1998) 2287.
76 Leiter F H, Alves H R, Romanov N G, Hofmann D M & Meyer B K, *Phys B*, 201 (2003) 340.
77 Korsunska N O, Borkovska L V, Bulakh B M, Khomenkova L V, Kushnirenko V I & Markevich I V, *J Lumin*, 102 (2003) 733.
78 Oba F, Nishitani S R, Isotani S & Adachi H, *J Appl Phys*, 90 (2001) 824.
79 Yang Y H, Chen X Y, Feng Y & Yang G W, *Nano Lett*, 7 (2007) 3879.
80 Wang N W, Yang Y H & Yang G W, *J Phys Chem C*, 113 (2009) 15480.
81 Djuris˘ic A B & Leung Y H, *Small*, 2 (2006) 944.
82 Ahmed M A A, *Brno University of Technology*, (2004) 8.
83 Cullity B D, Reading, (1978) 102.
84 Bhaduri S B & Bhaduri S, Plenum, New York, 289 (1999) doi:10.1016/S1470-1804(99) 80057-1
85 Mazhdi M & Hossein Khani P, *Int J Nano Dimens*, 4 (2012) 233.
86 Kittel C, John Wiley & Sons, New York, (2005).
87 Gaudon M, Toulemonde O & Demourgues A, *Inorg Chem*, 46 (2007) 10996.
88 Prabhu Y T, Rao K V, Sai Kumar V S & Kumari B S, *Advances in Nanoparticles*, 2 (2013) 45.
89 Peiser H S, Rooksby H P & Wilson A J C (Institute of Physics, London) 1955.
90 Clark G L, Applied X-rays, (McGraw- Hill Book Company, New York) 1955.
91 Compton A H, Allison S K & Van D (Nostrand Company, New York) 1935.
92 Zak A K, Abrishami M E, Majid Abd W H, Yousefi R & Hosseini S M, *Ceram Inter*, 37 (2011) 393.
93 Khan Z R, Zulfequar M & Mohd Shahid K, 46 (2011) 5412.
94 Mott N F & Davis E A, (Calendron Press, Oxford), 1979.
95 Lin K F, Hsu H C, Lin L J & Hsieh W F, *Chem Phys Lett*, 409 (2005) 208.
96 Moloto N, Mpelane S, Sikhwivhilu L M Ray & S S, *Int J Photoenergy*, 2012 (2011) 189069.
97 Viswanatha R, Satpati B, Satyam P V, Dev B N & Sarma D D, *J Mat Chem*, 14 (2004) 661.
98 Virendra P, Charlnene D, Deepti Y, Shaikh A J & Nadanathangam V, *Spectrochimica Acta Part A*, 65 (2006) 173.